22nd International Congress on X-Ray Optics and Microanalysis IOP Publishing
Journal of Physics: Conference Series **499** (2014) 012006 doi:10.1088/1742-6596/499/1/012006

Edge illumination X-ray phase-contrast imaging: nanoradian sensitivity at synchrotrons and translation to conventional sources

P C Diemoz[1,2], M Endrizzi[1], C K Hagen[1], C Rau[3], A Bravin[4], R D Speller[1], I K Robinson[2,5] and A Olivo[1,2]

[1] Dept. of Medical Physics and Bioengineering, UCL, WC1E 6BT London, UK
[2] Research Complex at Harwell, Harwell Oxford Campus, OX11 0DE Didcot, UK
[3] Diamond Light Source, Harwell Oxford Campus, OX11 0FA Didcot, UK
[4] European Synchrotron Radiation Facility, 38043 Grenoble, France
[5] London Centre for Nanotechnology, WC1H 0AH London, UK

E-mail: p.diemoz@ucl.ac.uk

Abstract. Edge illumination is an X-ray phase-contrast imaging technique that can be efficiently applied to both synchrotron radiation and laboratory sources. Its implementation with these two types of setups is here described, and a recently developed method to perform quantitative retrieval of the object attenuation and refraction properties is presented. We report results obtained at two synchrotron radiation facilities and with one of the setups installed in our laboratories at University College London, which show that very high angular sensitivities can be obtained with this technique. The effect of different experimental parameters on the achievable sensitivity is also analyzed. The obtained results will be a useful guide for the design and optimization of future experimental layouts.

1. Introduction

X-ray phase-contrast imaging (XPCi) has been an important branch of X-ray research since the mid nineties [1-4]. The edge illumination (EI) XPCi technique, in particular, has emerged over the last years for its ability to combine high phase sensitivity with a practical and simple implementation [5-11]. EI was first developed and experimentally applied at the Elettra synchrotron radiation (SR) facility, by using a parallel and monochromatic beam [5]. The main idea behind its development was to reproduce the high angular selectivity obtainable with diffraction from a perfect crystal (like in the so-called analyzer-based XPCi technique [1]), however with a simpler setup that does not require a crystal.

Analyzer-based imaging (ABI) is a highly sensitive technique that has been also successfully applied to the imaging of several types of biomedical objects [12,13]. However, it requires strict monochromatization/collimation of the beam, therefore leading to inefficient use of the X-ray flux, and a high mechanical stability, since the crystal orientation has to be controlled with sub-μrad precision. This makes it an excellent tool at SR facilities, but one that is not readily adaptable to conventional x-ray sources.

The development of the EI method arose from the simple observation that a collimated beam is geometrically deflected in the presence of sample refraction, and this deviation can be converted, with a sufficiently large propagation distance, into a detectable spatial shift of the beam. The collimation requires only the use of a one-dimensional (1D) slit, while the displacement of the beam caused by refraction can be sensed by using an absorbing edge set in front of the detector, at a distance on the order of tens of centimetres or a few metres from the sample (figure 1a). The use of such a simple setup, as opposed to the diffraction from a perfect crystal, eliminates the need of a monochromatic beam and of a stringent control of the mechanical stability.

In recent years, the technique has been further developed at University College London (UCL) and its application to laboratory setups based on conventional X-ray tubes was demonstrated [6,7,10,11]. In order to exploit the full size of the two-dimensional (2D) beam, the sample and detector slits are replaced by two masks, made of multiple apertures alternated to absorbing septa (figure 1b). The period of the detector mask is designed so that it matches that of the detector pixels, while the period of the sample mask is calculated so as to account for the magnification caused by the beam divergence. This laboratory implementation of EI has been already successfully applied to the imaging of biological tissues, in particular ex-vivo cartilage and breast samples [14,15].

EI was demonstrated to effectively overcome most of the roadblocks that have so far prevented a widespread deployment of XPCi in standard laboratories, namely the requirements of other XPCi techniques in terms of either beam monochromaticity, small source dimensions, high setup stability, or large doses delivered to the sample. In fact, EI can be applied effectively even with relatively large source sizes, up to at least 100 μm, it is insensitive to broad beam polychromaticity, and robust to mechanical vibrations in the setup. Besides, since the beam is collimated before and not after the sample, unnecessary exposure of the sample is avoided and doses can be kept low (a detailed discussion of dose delivery in lab-based EI goes beyond the scope of this proceedings paper and can be found in [15]).

It should be noted that a more recent XPCi technique, grating interferometry (GI) [16,17], was also implemented with laboratory sources [18]. GI exploits the fractional Talbot effect from a diffraction grating to produce a modulation of the beam intensity: this pattern and the changes to it introduced by the sample are then sensed with the use of a second (absorption) grating placed just before the detector. The application with conventional sources requires the use of a third (absorption) grating near the source, which produces a plurality of self-coherent beamlets [18]. Although there exists a superficial similarity between the EI and GI experimental setups (both use phase or absorption masks/gratings), the physical principles at the basis of the two techniques and their practical implementation are different [19]. For example, one important distinctive feature we would like to mention here is the fact that GI exploits the fractional Talbot effect, which relies on high beam spatial and temporal coherence, while EI is a non-interferometric, intrinsically incoherent method, and can in fact be accurately described with the use of geometrical optics [11,20].

Quantitative retrieval of the object attenuation and refraction maps with EI has also been recently demonstrated, with both synchrotron and laboratory setups, and proven to provide highly accurate results [7,9,11]. Moreover, recent experiments performed at two SR facilities have shown that extremely high angular sensitivity is achievable with this method over a wide range of energies and experimental conditions [9]. The sensitivity of one of the laboratory setups installed at UCL has also been estimated and proven to be at least comparable to results obtained with other XPCi techniques, showing that the simplicity of the setup used by EI does not come at the price of a decreased sensitivity [11].

In the following sections, we describe the application of the EI method and derive a theoretical expression for the technique's sensitivity, dependent upon the used experimental parameters. We then report on some of the main results obtained in our recent experiments carried out at the European Synchrotron Radiation Facility (ESRF, France) and Diamond Light Source (Didcot, UK), and with our laboratory-based setup.

2. The EI technique and its angular sensitivity

As mentioned above, in the EI technique the beam is collimated by a 1D slit before hitting the sample, typically to a few µm or tens of µm, and then analyzed with the use of an absorbing edge (in practice, a slit) in contact with the detector (figure 1a). The adaptation of the method in the case of a spatially extended beam, like that provided by an X-ray tube, is simple, and only requires the use of a pair of sample and detector masks with appropriate periods and aperture sizes (figure 1b). In the normal implementation of EI, the setup is designed so that there is no cross-talk between each sample-detector aperture pair and the adjacent ones. Therefore, in the following we only consider the case of one sample and one detector aperture, as all aperture pairs are independent of the others and the same formalism therefore applies to all in exactly the same way.

The intensity incident on the detector, without the sample, depends on the relative position between each detector aperture and the corresponding beamlet incident on it. In particular, it can be written as the integral of the beam distribution S_{ref} (defined as the number of photons per unit distance), within the two edges of the aperture, i.e. $I_{ref}\left(x_e\right)=\int_{x_e}^{x_e+d} dx S_{ref}\left(x\right)=I_0 C\left(x_e\right)$. x_e is the position of the lower edge of the detector aperture, d its dimension, $I_0=\int_{-\infty}^{+\infty} dx S_{ref}\left(x\right)$ is the total intensity of the beam and $C\left(x_e\right)=I_0^{-1}\int_{x_e}^{x_e+d} dx S_{ref}\left(x\right)$ is the so-called illumination curve. The latter represents the fraction of the total beam that enters the aperture: it is a function comprised between 0, when the absorbing part of the mask is totally covering the beam, and a maximum value (close to 1), when the detector and sample apertures are perfectly aligned.

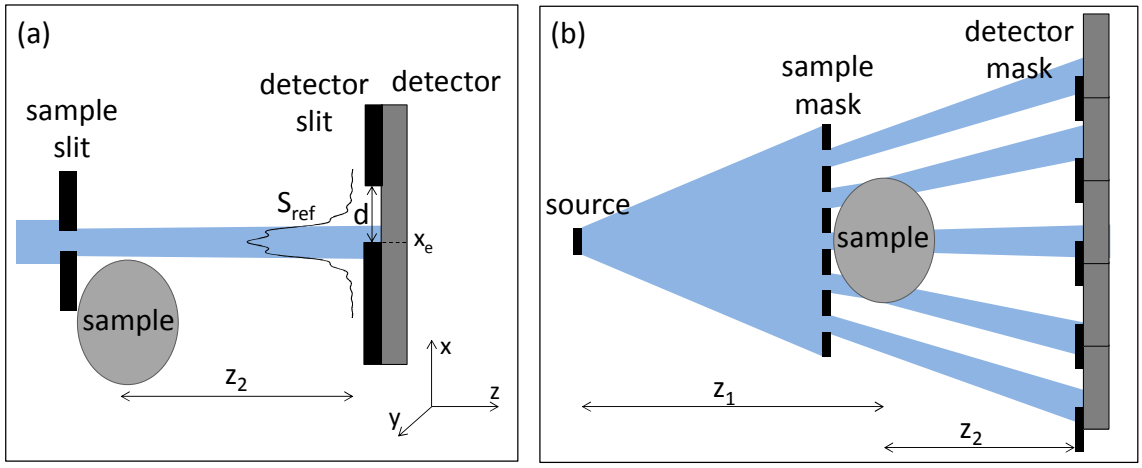

Figure 1. Schematic representation of the edge illumination setup, in the case of (a) a laminar beam and a single pair of sample and detector apertures and (b) a 2-dimensional beam and a pair of sample and detector masks (not to scale). The values of the experimental parameters vary depending on the targeted applications: values for the specific examples provided in this article are given in the text.

When the object is introduced, it can have two effects: beam attenuation, leading to an overall decrease in the beam intensity, and beam refraction (which for samples of interest is typically on the order of several nrad, up to a few µrad). The latter effect causes a spatial shift of the beam at the detector plane equal to $\Delta x = z_2 \Delta\theta_x$ (usually in the sub-µm range), where $\Delta\theta_x$ is the component of the refraction angle along the direction x perpendicular to the edge and z_2 is the sample-to detector edge distance.

Mathematically, the intensity on the detector can then be written as [9,11]:

$$I_{obj}\left(x_e\right) = I_0 T_{eff} C\left(x_e - z_2 \Delta\theta_{x,eff}\right) \tag{1}$$

where T_{eff} and $\Delta\theta_{x,eff}$ represent the effective beam transmission and refraction angle, calculated as a weighted average over the entire spectrum and the system response function [19]. If two images are acquired at different (arbitrary) positions of the detector aperture, $x_{e,+}$ and $x_{e,-}$, these two components can be separated and quantified (note that in the lab-based implementation of EI it is usually more advantageous to shift the sample mask instead of the detector mask, so that the detector can be kept in a fixed position). In particular, the refraction angle can be calculated by dividing pixel-by-pixel the two images:

$$\Delta\theta_{x,eff} = \frac{1}{z_2} R^{-1}\left(\frac{I_{obj,+}}{I_{obj,-}}\right) \tag{2}$$

where the function *R* is defined as:

$$R\left(z_2 \Delta\theta_{x,eff}\right) \equiv \frac{C\left(x_{e,+} - z_2 \Delta\theta_{x,eff}\right)}{C\left(x_{e,-} - z_2 \Delta\theta_{x,eff}\right)} \tag{3}$$

and its shape can be computed numerically using the experimental measure of the illumination curve *C*.

Equation (2) can also be used to estimate, from the noise of the two input images, the uncertainty on the retrieved values of $\Delta\theta_{x,eff}$. Under the assumption of pure statistical noise, in fact, it is possible to demonstrate that [11]:

$$\sigma\left(\Delta\theta_{x,eff}\right) \simeq \frac{\sqrt{C\left(x_{e,+}\right)}}{z_2\sqrt{2TI_0}\left[S_{ref,n}\left(x_{e,+}\right) - S_{ref,n}\left(x_{e,+} + d\right)\right]} \tag{4}$$

where $S_{ref,n} \equiv I_0^{-1} S_{ref}$ is the beam normalized spatial distribution, and where we have assumed that symmetric mask positions are used for the two input images (i.e. the detector mask is shifted with respect to the sample mask of the same amount in each direction). The amplitude of the noise in the refraction image, calculated from equation (4), is a precise indication of the angular sensitivity of an EI setup. In fact, only angles that are larger than the noise level are effectively detectable by the imaging system.

The noise in the processed image, in turn, does not only depend on the noise in the input images, but also on the characteristics of the experimental setup, which define how much the sample refraction is "amplified" to provide the final image signal. In particular, it can be seen from equation (4) that the noise in the refraction image depends upon several setup parameters, including the fraction of the beam falling within the detector aperture (the level of illumination *C*), the propagation distance and the value of the beam distribution at the two edges of the aperture. This last dependence can be explained in an intuitive way by taking figure 1a as a reference. When the beam is shifted, the number of gained (or lost) photons on the detector, at the lower edge of the aperture, is equal to $\pm\Delta x \cdot S_{ref}\left(x_{e,+}\right)$ (in the small angle approximation). This quantity, however, is partially compensated by the beam lost (or gained) at the edge at the other side of the aperture, i.e. $\mp\Delta x \cdot S_{ref}\left(x_{e,+} + d\right)$. This shows how the dimension of the detector aperture is also an important parameter in the design of an EI setup. In particular, if its size is too small compared to the beam width, then $S_{ref}\left(x_{e,+} + d\right)$ is not negligible,

and can negatively affect the amplitude of the detected signal. On the other hand, the period of the masks does not affect the sensitivity, as long as it is large enough to prevent beam spillover between adjacent aperture pairs.

It can be shown [11] that, for a sufficiently large projected source size, the beam distribution can be very well approximated by the geometrical optics (i.e. neglecting the wave properties of the beam and assuming that photons travel along straight lines). In this case, it is simply given by the convolution between the sample aperture projected onto the detector plane and the projected source size. An important consequence of this is that the beam shape has no dependence upon energy. In other words, the optical elements of the setup can be considered to be achromatic.

In order to exemplify the effect of some key geometrical parameters of the setup on the achievable sensitivity, we present in the following the calculation (based on equation (4)) of the relative sensitivity for a variety of different system configurations. Initially, we consider the parameters of one of our lab-based experimental setups: source-to-sample distance z_1 = 1.6 m, z_2 = 0.4 m, sample aperture a = 12 µm, detector aperture d = 20 µm. The misalignment between the masks is set to a 50% level (with, alternatively, the lower or upper edge of the detector aperture being aligned with the centre of the sample aperture for the two input images). While in our current setup the full width at half maximum (FWHM) of the source is about 70 µm, we vary it continuously in the simulation results shown in figure 2, in order to elucidate its effect on the signal amplitude. The calculation is repeated by using smaller (8 µm) and larger (20 µm) sample apertures. In all cases, the sensitivity is constant (at the maximum value) when the projected source size is smaller than the aperture, as in this case the width of each beamlet incident on the detector mask is determined primarily by the aperture size. The sensitivity decreases, instead, when the source starts to dominate over the aperture size. However, this decrease is slow, and even at relatively large source sizes (for example at the value of 70 µm used by our setup) most of the phase sensitivity is still preserved with respect to the ideal case of a point source. When the sample aperture is made narrower, the "plateau" is smaller, but the initial sensitivity is higher as the beam is sharper. The opposite happens when a larger sample aperture is considered.

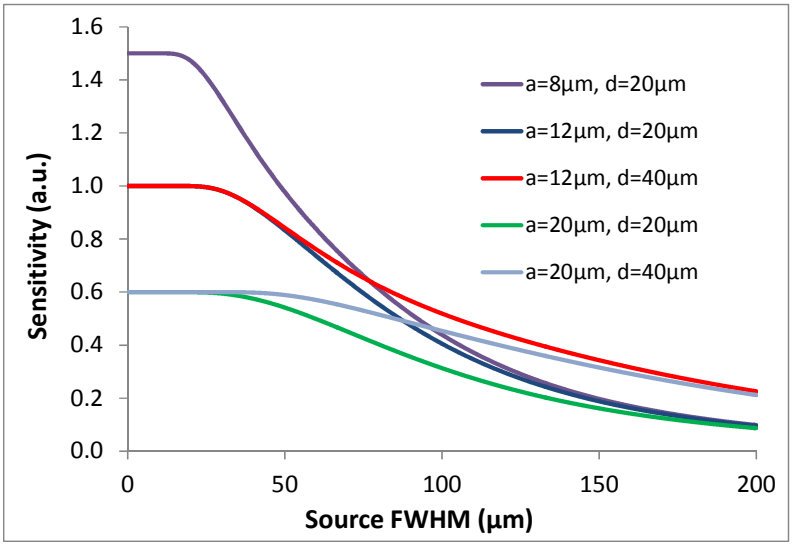

Figure 2. Dependence of the sensitivity upon the dimension of the X-ray source. Curves are calculated using equation (4) for different values of the sample aperture (a) and of the detector aperture (d) (see text for the values of the other experimental parameters).

It is possible to show that part of the signal decrease at large source sizes is actually due to the presence of the second edge of the detector aperture. In fact, in this case the beam incident on it

becomes larger than the detector aperture itself. As a consequence, the value of the beam at the upper edge is not negligible, and this leads to a decrease of the signal as discussed above (cf. equation (4)). In order to prove this, we recalculated the sensitivities at a=12 μm and a=20 μm using aperture dimensions increased to d=40 μm. The sensitivity at large source sizes is now drastically improved (see figure 2).

3. Experimental application of EI to synchrotron and laboratory setups

The implementation of the EI technique at SR facilities presents some differences compared to that with a laboratory source. In particular, thanks to the very large source-to-sample distance (sometimes > 100 m), the sample-to-detector distance can be considerably increased (up to several meters), without this making the projected source size (and consequently the beamlet) excessively large [8,9]. As a consequence, the sensitivity can be strongly improved (cf. equation (4)). In addition, since the beam shape is laminar, only one pair of sample and detector slits is usually employed.

The technique was applied using a very high X-ray energy (85 keV) at the ID17 beamline of the ESRF, and using low energy (12 keV) at the I13 beamline (coherent branch) of Diamond. The propagation distances were 6.0 m and 14.7 m, respectively. The aim of these experiments was double: to prove the applicability of EI over a broad energy range, and to experimentally demonstrate that very high sensitivity can be obtained, regardless of the specific characteristics of a given beamline. The experiments proved indeed very high angular resolutions, with a noise in the refraction image of less than 2 nrad with the first setup and of about 15 nrad with the second [9]. This represented a considerable improvement (of up to one order of magnitude better sensitivity) compared to values previously published for other XPCi techniques [9].

The difference between the values obtained in the ESRF and Diamond experiments was due to two main reasons: a higher photon statistics used in the ESRF setup, and a larger broadening of the beam in the Diamond setup, which slightly decreases the sensitivity. The latter effect is due to the beam diffraction, which is not negligible when the projected source size is small, and is more important at lower energies. A consequence of this is that, in SR implementations, the setup can no more be considered achromatic as in the laboratory case.

As an example of the image quality achievable instead in a non-ideal laboratory setup, a refraction image of a wasp, calculated using equation (2), is reported in figure 3. It was obtained using the setup described in the previous section, which is installed in the Radiation Physics laboratories at UCL. The periods of the sample and detector masks are 66.8 μm and 83.5 μm, respectively, while the aperture sizes are 12 μm and 20 μm (more details on the masks design can be found in [11]). The apertures are oriented in the vertical direction, so that the setup is sensitive to beam deflections in the horizontal plane. The two images used as input for the phase retrieval were acquired with a 50% misalignment between the two masks, respectively in the positive and negative directions, at a tube voltage of 35 kVp and with an exposure time of 7 s each. It should be noted that, although the 50% misalignment leads to X-rays intercepted by the detector mask and therefore to a dose increase, this can be avoided by reducing the apertures in the pre-sample mask, as described in [15]. The detector was the ANRAD 'SMAM' amorphous selenium flat panel, with a pixel size of 85 μm. In order to improve the spatial resolution, 8 dithering steps were performed, i.e. the image acquisition was repeated 8 times, each with a sub-period displacement of the sample in the horizontal direction [21] (note that, if a resolution corresponding to the pixel size is already considered to be sufficient, there is no need for any sample dithering, i.e. the sample is not moved at all). The high angular resolution obtained is demonstrated by the detection of faint details in the insect, as for example the structures of the wasp wings and of the chest (figure 3).

The angular sensitivity of this system was estimated as the standard deviation of the values in large regions (500 x 100 pixels^2, outside the sample) of the refraction map. This calculation gave a value of 270±5 nrad, highly homogeneous over the entire field of view [11]. Furthermore, similar calculations performed for other images gave perfectly consistent results.

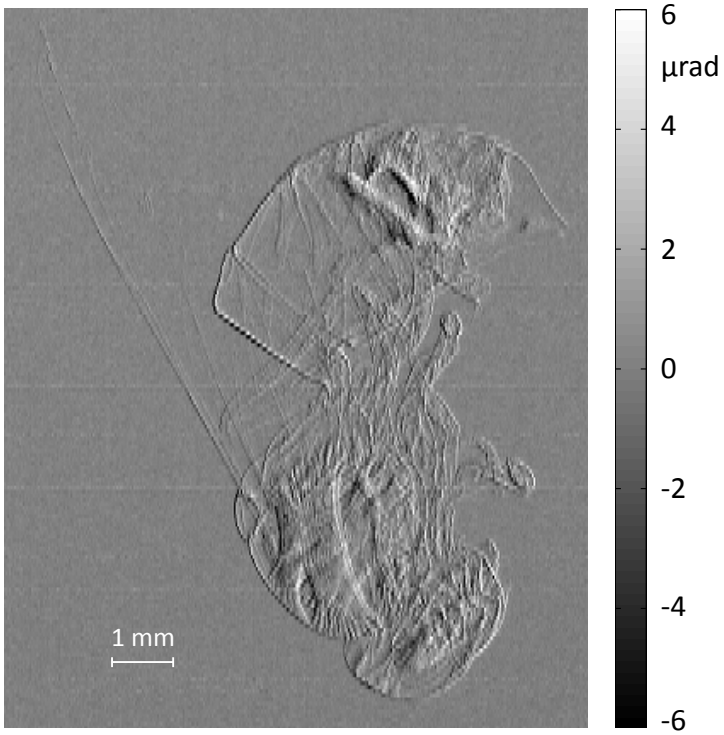

Figure 3. Edge illumination refraction image of a wasp, obtained with our laboratory-based setup (details in text).

The obtained sensitivity is comparable with values previously published for GI. Different implementations of the latter method, in fact, provided sensitivities varying from 100 to 700 nrad [22-24]. However, in these cases, a series of at least 12 images were acquired in order to perform the phase retrieval, instead of only two required by our method when dithering is not needed. Note that the only purpose of sample dithering is to increase the object sampling rate i.e. the spatial resolution, while it has no effect whatsoever on the noise properties and the sensitivity, as the photon statistics in each pixel of the final image is not increased [21]. Conversely, in the case of the 12 "phase stepping" images used in GI, these all contribute to the statistics in the final, processed image, thus reducing the noise approximately by a factor $\sqrt{12}$. Considering that phase sensitivity is defined (here and elsewhere, e.g. [23, 24]) as the standard deviation of the measured angle, it is clear that this is directly influenced by the detected statistics. For example, the best result reported for GI (approximately 110 nrad, [22]) was obtained with 12 phase steps, i.e. by acquiring 12 images with an exposure time of 6.7 s each. By dividing our value of 270 nrad by $\sqrt{6}$ (ratio between the 12 images used in [22] and the 2 used by us, practically with the same exposure time), one obtains roughly 110 nrad, i.e. practically an exact match with the results obtained with GI.

These results demonstrate that, despite the simplicity and practicality of our setup, high angular resolution is obtainable. Besides, we would like to underline the high robustness of the setup with respect to mechanical stability. Environmental vibrations up to a few µm were in fact measured in our laboratory, however these did not affect the quality and the quantitative accuracy of the obtained images. This increased stability is a direct consequence of the large pitch of our masks: it was first observed in the original embodiments of the laboratory prototypes [25], and was recently discussed in more detail [10].

4. Conclusions

The EI method has been successfully applied to both synchrotron and laboratory setups. It was proven to yield unprecedented angular resolution at synchrotrons, thanks to the possibility of using very large propagation distances, on the order of 5-15 m: this enables the amplification of very small refraction angles, which are converted into a detectable displacement of the beam at the detector level. Furthermore, the technique was demonstrated to be efficiently applicable over a broad range of X-ray energies, thus allowing studying a wide variety of different samples.

Thanks to its robustness against increased source dimensions, and to its insensitivity to the beam polychromaticity, EI is also compatible with the use of conventional X-ray tubes. Other key advantages of this setup are the possibility of using very large fields of view, as large masks up to several centimetres can be manufactured, and its resilience to mechanical vibrations. The latter point is particularly important in view of the potential application of the method in normal laboratories and ultimately to clinics. It is also advantageous for the accuracy of the image reconstruction in the cases when more than one image needs to be acquired and processed, like in computed tomography or when phase retrieval is performed.

The implementation of the method in both synchrotron and laboratory setups was discussed, and we have reported on the angular sensitivities obtained in these cases. We have also studied theoretically the dependence of the sensitivity upon various experimental parameters, and in particular the effects of the source dimension, and sample and detector apertures. The developed formalism and the highlighted dependences on the parameters will be key in the design and optimization of future experimental EI setups.

Acknowledgements

This work was supported by the UK Engineering and Physical Sciences Research Council (Grant Nos. EP/G004250/1 and EP/I021884/1). M.E. and P.C.D. are supported by Marie Curie Career Integration Grant Nos. PCIG12-GA-2012-334056 and PCIG12-GA-2012-333990 within the Seventh Framework Programme of the European Union.

References

[1] Ingal V N and Beliaevskaya E A 1995 *J. Phys. D* **28** 2314-7
[2] Snigirev A, Snigireva I, Kohn V, Kuznetsov S and Schelokov I 1995 *Rev. Sci. Instrum.* **66** 5486-92
[3] Wilkins S W, Gureyev T E, Gao D, Pogany A and Stevenson W 1996 *Nature* **384** 35-8
[4] Momose A, Takeda T, Itai Y and Hirano K 1996 *Nat. Med.* **2** 473–5
[5] Olivo A *et al.* 2001 *Med. Phys.* **28** 1610-9
[6] Olivo A and Speller R D 2007 *Appl. Phys. Lett.* **91** 074106
[7] Munro P R T, Ignatyev K, Speller R D and Olivo A 2012 *Proc. Natl. Acad. Sci. USA* **109** 13922-7
[8] Olivo A, Diemoz P C and Bravin A 2012 *Opt. Letters* **37** 915-7
[9] Diemoz P C, Endrizzi M, Zapata C E, Pešić Z D, Rau C, Bravin A, Robinson I K and Olivo A 2013 *Phys. Rev. Lett.* **110** 138105
[10] Millard T P, Endrizzi M, Ignatyev K, Hagen C K, Munro P R T, Speller R D and Olivo A 2013 *Rev. Sci. Instrum.* **84** 083702
[11] Diemoz P C, Hagen C K, Endrizzi M and Olivo A 2013 *Appl. Phys. Lett.* **103** 244104
[12] Coan P, Bamberg F, Diemoz P C, Bravin A, Timpert K, Mutzel E, Raya J G, Adam-Neumair S, Reiser M F and Glaser C 2010 *Invest. Radiol.* **45** 437-44
[13] Zhao Y *et al.* 2012 *Proc. Natl. Acad. Sci. USA* **109** 18290-4
[14] Marenzana M, Hagen C K, Das Neves Borges P, Endrizzi M, Szafraniec M B, Ignatyev K and Olivo A 2012 *Phys. Med. Biol.* **57** 8173-84
[15] Olivo A *et al.* 2013 *Med. Phys.* **40** 090701

[16] David C, Nöhammer B, Solak H and Ziegler E 2002 *Appl. Phys. Lett.* **81** 3287-9
[17] Momose A, Kawamoto S, Koyama I, Hamaishi Y, Takai K and Suzuki Y 2003 *Jpn. J. Appl. Phys.* **42** L866-8
[18] Pfeiffer F, Weitkamp T, Bunk O and David C 2006 *Nat. Phys.* **2** 258-61
[19] Munro P R T and Olivo A 2013 *Phys. Rev. A* **87** 053838
[20] Munro P R T, Ignatyev K, Speller R D and Olivo A 2010 *Opt. Express* **18** 4103-17
[21] Ignatyev K, Munro P R T, Speller R D and Olivo A 2011 *Rev. Sci. Instrum.* **82** 073702
[22] Revol V, Kottler C, Kaufmann R, Straumann U and Urban C 2010 *Rev. Sci. Instrum.* **81** 073709
[23] Thüring T, Modregger P, Hämmerle S, Weiss S, Nüesch J and Stampanoni M 2012 *AIP Conf. Proc.* **1466**, 293-8
[24] Thüring T, Hämmerle S, Weiss S, Nüesch J, Meiser J, Mohr J, David C and Stampanoni M 2013 *Proc. of SPIE* **8668** 866813
[25] Olivo A, Ignatyev K, Munro P R T and Speller R D 2011 *Appl. Opt.* **50** 1765-9